arXiv:1202.5834v1 [hep-lat] 27 Feb 2012

Preliminary lattice QCD calculation of the σ meson decay width

Ziwen Fu
Key Laboratory of Radiation Physics and Technology (Sichuan University), *Ministry of Education;*
Institute of Nuclear Science and Technology, Sichuan University, Chengdu 610064, P. R. China.

We present an exploratory lattice QCD calculation of the σ meson decay width using the s-wave scattering phase shift for the isospin $I = 0$ pion-pion ($\pi\pi$) system. The finite size formula developed by Rummukainen and Gottlieb is employed to estimate the phase shift, which demonstrates a characteristic consistent with the presence of a resonance around σ meson mass. The effective range formula is adopted to describe the phase-shift dependence, and we extract the effective $\sigma \to \pi\pi$ coupling constant $g_{\sigma\pi\pi} = 2.69(44)$ GeV, which is consistent with the theoretical predictions. The decay width estimated from phase shift is about 236 ± 49 MeV. Our preliminary lattice simulations are carried out with MILC full QCD gauge configurations in the presence of $2 + 1$ flavors of the "Asqtad" improved staggered dynamical sea quarks on a $16^3 \times 48$ lattice at $m_\pi/m_\sigma \approx 0.414$ and lattice spacing $a \approx 0.15$ fm.

PACS numbers: 12.38.Gc, 11.15.Ha

I. INTRODUCTION

It is well-known that sigma meson is a resonance, which is a state with a considerable decay width under strong interactions, and decay via strong interaction. In 2010, Particle Data Group (PDG) [1] lists the meson $f_0(600)$, which is usually called σ meson ($J^{PC} = 0^{++}$, $I = 0$), with an estimated mass ($400 - 1200$ MeV) and an estimated decay width ($600 - 1000$ MeV). Such a low-lying scalar meson has been known to play a significant role in nuclear and hadron physics. The existence of the σ meson has been established by some refinement of experimental analyses [2–11] and some phenomenological studies [12–21]. The Dalitz plot analysis of Fermilab experiment E791 [7] yields its decay width about $324^{+42}_{-40} \pm 21$ MeV. Moreover, the σ meson has been extensively studied with BES data [3, 4], and the most recent analysis based on the events collected by BESII gives the pole position of to be σ $(541 \pm 39) + i(252 \pm 42)$ MeV [3].

Although the direct determination of the σ resonance parameters from QCD is afflicted with the fundamental difficulties since the calculation of resonance masses and decay widths is essentially a nonperturbative problem. Several research groups have undertaken theoretical efforts to study the σ meson and its resonance parameters [12–21]. Originally the σ-meson was introduced to fit experimental data and its mass was chosen to reproduce the experimental results. There is a wide variety for defining the mass and width of a particle. Some authors use the pole approach with the mass and width of resonance taken from the position of the pole of the T-matrix [19]. Another way to study the mass and width of resonances is through the use of the spectral function [20]. However, all the experimental and theoretical analyses give a little bit different resonance mass and decay width for σ meson. Therefore, there is not close to the consensus yet on its resonance parameters.

The most feasible way to extract σ resonance parameters nonperturbatively from first principles is the use of lattice QCD. The dominant σ decay channel is to a pair of pions, which can be precisely handled on the lattice. Until now, no direct lattice QCD study about σ resonance have been reported, possibly because the rectangular and vacuum diagram are extremely difficult to reliably calculate. Inspired by J. Nebreda and J. Pelaezet's theoretical studies on σ resonance [22], our previous works about the precise extraction of σ mass [23], our reliable extraction of the $\pi\pi$ scattering length at the $I = 0$ channel [24], and our preliminary lattice QCD calculation of κ meson decay width [25, 26], in this work, we further explore its resonance parameters directly from lattice QCD.

In the present study, we estimate the σ decay width by calculating the s-wave scattering phase shift for the $I = 0$ $\pi\pi$ system. We discuss the ground state of the $I = 0$ $\pi\pi$ system with the total zero momentum in center of mass (CM) frame, and the non-zero momentum in the moving frame (MF). The calculations are carried out with MILC full QCD gauge configurations in the presence of $2 + 1$ flavors of the Asqtad improved staggered dynamical sea quarks, generated by the MILC collaboration [27, 28]. The meson masses were determined from our previous spectrum analysis [23] which gave $m_\pi/m_\sigma \approx 0.414$, and the lattice parameters were determined by the MILC collaboration, namely, the lattice extent L is about 2.5 fm and the lattice space inverse $1/a = 1.358$ GeV [27, 28]. The finite size formula [29–33] is employed to the $\pi\pi$ system in the moving frame, and we utilize the Rummukainen-Gottlieb formula [34], which is the extension of the Lüscher formula to the moving frame, to estimate the s-wave phase shift. This calculation is carried out at two energies which enable us to investigate the existence of the σ resonance.

This paper is organized as follows. In Sec. II we discuss our calculation method. In Sec. III, we show the simulation parameters and our concrete lattice calculations. We present our lattice simulation results in Sec. IV. Our conclusions and outlooks are given in Sec. V.

II. METHODS

A. Scattering phase

In the $\pi\pi$ system, the relativistic Breit-Wigner formula (RBWF) for the elastic s-wave scattering amplitude a_0 in the resonance region with a center-of-mass energy m_σ and a decay width Γ_R reads [1]

$$a_0 = \frac{-\sqrt{s}\,\Gamma_R(s)}{s - m_\sigma^2 + i\sqrt{s}\,\Gamma_R(s)}\,, \tag{1}$$

where $s = E_{CM}^2$ is the invariant mass of the $\pi\pi$ system, E_{CM} is the center-of-mass energy, and a_0 is related to the s-wave scattering phase δ_0 through $a_0 = (e^{2i\delta_0} - 1)/2i$. The RBWF can be conveniently expressed as

$$\tan\delta_0 = \frac{\sqrt{s}\,\Gamma_R(s)}{m_\sigma^2 - s}\,. \tag{2}$$

The σ resonance has quantum numbers $I(J^P) = 0(0^+)$ and decays into two pions in the s-wave. The decay width $\Gamma_R(s)$ can be written in terms of the effective $\sigma \to \pi\pi$ coupling constant $g_{\sigma\pi\pi}$ [22],

$$\Gamma_R(s) = \frac{g_{\sigma\pi\pi}^2}{8\pi}\frac{p}{s}, \tag{3}$$

where $p = \sqrt{s/4 - m_\pi^2}$ is the center-of-mass momentum of the pion. With a combination of Eqs. (2) and (3), a description of the scattering phase shift in the s-wave as a function of the $\sqrt{s}$ is provided by so-called the effective range formula (ERF) in the elastic region, namely,

$$\tan\delta_0 = \frac{g_{\sigma\pi\pi}^2}{8\pi}\frac{p}{\sqrt{s}(m_\sigma^2 - s)}. \tag{4}$$

This equation allows us a linear fit or solving for two unknown parameters: coupling constant $g_{\sigma\pi\pi}$ and the resonance position m_σ.

It should be stressed that we will use the ERF to solve the scattering phase shifts which are measured by our lattice simulations, where we even used the pion mass which are larger than its physical ones.

The σ decay width Γ_σ can then be calculated through,

$$\begin{aligned} \Gamma_\sigma &= \Gamma_R(s)\Big|_{s=m_\sigma^2} = \frac{g_{\sigma\pi\pi}^2}{8\pi}\frac{p_\sigma}{m_\sigma^2}\,, \\ p_\sigma &= \sqrt{m_\sigma^2/4 - m_\pi^2}\,. \end{aligned} \tag{5}$$

Therefore, Eqs. (4) and (5) allow us to extract m_σ and Γ_σ through the dependence of the s-wave $\pi\pi$ scattering phase shift δ_0 on the invariant mass s.

B. Finite-volume method

A calculation of the phase shift from lattice QCD is practicable by using the finite-size formula proposed by Lüscher [29–33]. In this method, the phase shift is extracted from the energy eigenvalues of the $\pi\pi$ system enclosed in a cubic box with spatial extension L. In this work, we focus on the σ meson decay into two pions in the s-wave, and only consider the $\pi\pi$ system with the isospin representation of $(I, I_z) = (0, 0)$.

1. Center of mass frame

In the center-of-mass frame, when the σ meson is at rest, the possible energy eigenvalues of the noninteracting $\pi\pi$ system are given by

$$E = 2\sqrt{m_\pi^2 + p^2}\,, \tag{6}$$

where $p = |\mathbf{p}|$, $\mathbf{p} = (2\pi/L)\mathbf{n}$, and $\mathbf{n} \in \mathbb{Z}^3$. In a typical lattice simulation, this energy for $\mathbf{n} \neq 0$ is much larger than the sigma mass m_σ. For example, on our full QCD configurations, the lowest energy for $\mathbf{n} \neq 0$ calculated from m_π and m_σ determined in our previous study [23], is $E = 1.56 \times m_\sigma$, which is obviously away from the resonance, and thus it is not eligible to study the σ meson decay. Thus, we only consider the dominant low energy states, namely, $\mathbf{n} = 0$ case, where pions and σ meson are at zero momentum. The energies of these states are

$$\begin{aligned} E_1 &= 2m_\pi \quad \text{for } \pi\pi \text{ system}, \\ E_2 &= m_\sigma \quad \text{for } \sigma \text{ meson}\,. \end{aligned} \tag{7}$$

On our full QCD configurations the invariant mass of two free pions takes $\sqrt{s} = 0.828 \times m_\sigma$, which is still a little bit away from the resonance mass m_σ, but closer to m_σ than those with $\mathbf{n} \neq 0$.

In the interacting case, the total momentum of the $\pi\pi$ system is also zero. The energy eigenvalues are shifted by the hadronic interaction from E_n to $\overline{E}_n$ $(n = 1, 2)$, and the energy eigenvalue for $\pi\pi$ system is given by,

$$\overline{E} = 2\sqrt{m_\pi^2 + k^2}\,, \quad k = \frac{2\pi}{L}q\,, \tag{8}$$

where q is no longer required to be a integer. In this work, we restrict on the energy eigenstates with energies $\overline{E}$ in the elastic region $2m_\pi < \overline{E} < 4m_\pi$ with $\pi\pi$ system having the same quantum numbers as σ meson. In the center-of-mass frame these energy eigenstates transform under the cubic group O_h in the irreducible representation $\Gamma = T_1^+$. The finite-size formula relating the energy $\overline{E}_n$ to the scattering phase shift δ_0 is [29–33]

$$\tan\delta_0(k) = \frac{\pi^{3/2}q}{\mathcal{Z}_{00}(1; q^2)}\,, \tag{9}$$

where the zeta function denoted by

$$\mathcal{Z}_{00}(s; q^2) = \frac{1}{\sqrt{4\pi}}\sum_{\mathbf{n}\in\mathbb{Z}^3}\frac{1}{\left(|\mathbf{n}|^2 - q^2\right)^s}\,. \tag{10}$$

The expansion of the zeta function in Eq. (10) is convergent only when Re $s > 3/2$, but it can be analytically continued to $s = 1$. $\mathcal{Z}_{00}(s; q^2)$ can be efficiently evaluated by the method described in Appendix A of Ref. [35].

2. Moving frame

In order to realize the energy of the $\pi\pi$ system is more close to the sigma mass m_σ, we consider a system having a non-zero total momentum, namely, the moving frame [34]. Using a moving frame with total momentum $\mathbf{P} = (2\pi/L)\mathbf{d}$, $\mathbf{d} \in \mathbb{Z}^3$, the energy eigenvalues for non-interacting $\pi\pi$ system are

$$E_{MF} = \sqrt{m_\pi^2 + p_1^2} + \sqrt{m_\pi^2 + p_2^2}, \qquad (11)$$

where $p_1 = |\mathbf{p}_1|$, and $\mathbf{p}_1$, $\mathbf{p}_2$ denote the three-momenta of the pions, which satisfy the relations,

$$\mathbf{p}_i = \frac{2\pi}{L}\mathbf{n}_i\,, \quad \mathbf{n}_i \in \mathbb{Z}^3\,, \quad \mathbf{P} = \mathbf{p}_1 + \mathbf{p}_2. \qquad (12)$$

In the center-of-mass frame, the value of the E_{CM} is directly given by the discrete energy eigenvalue extracted from the large time behavior of the corresponding correlation function. The relativistic 4-momentum squared is invariant, and E_{CM} is related to E_{MF} in the moving frame through the Lorentz transformation

$$E_{CM}^2 = E_{MF}^2 - \mathbf{P}^2\,. \qquad (13)$$

In the moving frame, the center-of-mass is moving with a velocity of $\mathbf{v} = \mathbf{P}/E_{MF}$. Using the standard Lorentz transformation with a boost factor $\gamma = 1/\sqrt{1-\mathbf{v}^2}$, the E_{CM} can be obtained through

$$E_{CM} = \gamma^{-1}E_{MF} = 2\sqrt{m_\pi^2 + p^{*2}}\,, \qquad (14)$$

where, in the center-of-mass frame, the total center-of-mass momentum vanishes, namely,

$$p^* = |\mathbf{p}^*|\,, \quad \mathbf{p}^* = \mathbf{p}_1^* = -\mathbf{p}_2^* = \frac{1}{2}\vec{\gamma}^{-1}(\mathbf{p}_1 - \mathbf{p}_2), \qquad (15)$$

here and later we denote the center-of-mass momenta with an asterisk (*), the boost factor acts in the direction of $\mathbf{v}$, and we use the shorthand notation

$$\vec{\gamma}^{-1}\mathbf{p} = \gamma^{-1}\mathbf{p}_\parallel + \mathbf{p}_\perp, \qquad (16)$$

where $\mathbf{p}_\parallel$ and $\mathbf{p}_\perp$ are the components of $\mathbf{p}$ parallel and perpendicular to $\mathbf{v}$, namely, $\mathbf{p}_\parallel = (\mathbf{p}\cdot\mathbf{v})\mathbf{v}/|\mathbf{v}|^2$, and $\mathbf{p}_\perp = \mathbf{p} - \mathbf{p}_\parallel$. From inspecting Eqs. (12) and (15), we can note that the $\mathbf{p}^*$ are quantized to the values

$$\mathbf{p}^* = \frac{2\pi}{L}\mathbf{r}\,, \qquad \mathbf{r} \in P_{\mathbf{d}}\,, \qquad (17)$$

where the set $P_{\mathbf{d}}$ is

$$P_{\mathbf{d}} = \left\{ \mathbf{r} \,\middle|\, \mathbf{r} = \vec{\gamma}^{-1}\left(\mathbf{n} + \frac{1}{2}\mathbf{d}\right),\ \ \mathbf{n} \in \mathbb{Z}^3 \right\}, \qquad (18)$$

In this work, we only consider the dominant low energy states in the moving frame, which are one pion with zero momentum, and one pion with the momentum $\mathbf{p} = (2\pi/L)\mathbf{e}_3$ ($\mathbf{d} = \mathbf{e}_3$) and σ meson with the momentum $\mathbf{P} = \mathbf{p}$. The energy eigenvalues of these states are

$$\begin{aligned} E_1 &= m_\pi + \sqrt{m_\pi^2 + p^2} && \text{for } \pi\pi \text{ system}, \\ E_2 &= \sqrt{m_\sigma^2 + P^2} && \text{for } \sigma \text{ meson}, \end{aligned} \qquad (19)$$

where $P = |\mathbf{P}|$. On our full QCD configurations the invariant mass of the $\pi\pi$ system takes $\sqrt{s} = 0.994 \times m_\sigma$, which is much closer to σ mass m_σ than that with total zero momentum in the center-of-mass frame. Therefore, we will only consider this case. The invariant mass $\sqrt{s}$ was evaluated from $\sqrt{s} = \sqrt{E_{MF}^2 - P^2}$.

In the interacting case, the $\overline{E}_{CM}$ is given by

$$\overline{E}_{CM} = 2\sqrt{m_\pi^2 + k^2}, \quad k = \frac{2\pi}{L}q. \qquad (20)$$

where q is no longer required to be a integer. It is exactly this energy shift between the non-interacting situation and the interacting case, namely, $\overline{E}_{CM} - E_{CM}$, that we can extract the $\pi\pi$ scattering phase. In this work, we only consider one moving frame, namely, $\mathbf{d} = \mathbf{e}_3$, where the energy eigenstates transform under the tetragonal group D_{4h}. The irreducible representation A_2^- is relevant for the $\pi\pi$ scattering states in the infinite volume. We calculate the energies associated with A_2^- sector. The hadron interaction shifts the energy from E_n to $\overline{E}_n$ ($n = 1, 2$), and the energies $\overline{E}_n$ are related to the $\pi\pi$ scattering phase shift δ_0 in the infinite volume through the Rummukainen-Gottlieb formula [34], namely,

$$\tan\delta_0(k) = \frac{\gamma\pi^{3/2}q}{\mathcal{Z}_{00}^{\mathbf{d}}(1;q^2)}\,, \qquad (21)$$

where we assume that the phase shifts δ_1 with $l = 2, 4, 6, ...$ are negligible in the energy range of interest, and the zeta function is formally defined by

$$Z_{00}^{\mathbf{d}}(s;q^2) = \sum_{\mathbf{r}\in P_{\mathrm{d}}} \frac{1}{(|\mathbf{r}|^2 - q^2)^s}, \qquad (22)$$

and the set $P_{\mathbf{d}}$ is denoted in Eq. (18). The zeta function converges when $\mathrm{Re}\, 2s > l+3$, and can be analytically continued to whole complex plane. The k is the momentum defined from the invariant mass $\sqrt{s}$ as $\sqrt{s} = 2\sqrt{k^2 + m_\pi^2}$. The calculation method of $Z_{00}^{\mathbf{d}}(1;q^2)$ is discussed in Appendix A of Ref. [35]. We also discussed it in Ref. [25], where we extend it to more general case. Using Eq. (22), we can obtain the phase shift from the energy eigenvalue calculated in the lattice simulations.

C. Correlation matrix

In the center-of-mass frame, the value of the E_{CM} is directly obtained by the discrete energy eigenvalue extracted from the correlation function at large time t. E_{CM} is related to E_{MF} through the Lorentz transformation

$$E_{CM}^2 = E_{MF}^2 - \mathbf{P}^2\,. \qquad (23)$$

To calculate two energy eigenstates, i.e., $\overline{E}_n$ $(n=1,2)$, we build a matrix of the time correlation function,

$$C(t) = \begin{pmatrix} \langle 0|\mathcal{O}_{\pi\pi}^\dagger(t)\mathcal{O}_{\pi\pi}(0)|0\rangle & \langle 0|\mathcal{O}_{\pi\pi}^\dagger(t)\mathcal{O}_{\sigma}(0)|0\rangle \\ \langle 0|\mathcal{O}_{\sigma}^\dagger(t)\mathcal{O}_{\pi\pi}(0)|0\rangle & \langle 0|\mathcal{O}_{\sigma}^\dagger(t)\mathcal{O}_{\sigma}(0)|0\rangle \end{pmatrix}, \tag{24}$$

where $\mathcal{O}_\sigma(t)$ is an interpolating operator for the σ meson with the definite momentum, and $\mathcal{O}_{\pi\pi}(t)$ is an interpolating operator for the $\pi\pi$ system with specified momentum. The interpolating operators $\mathcal{O}_\sigma(t)$ and $\mathcal{O}_{\pi\pi}(t)$ employed here is exactly the same as in our previous studies in Refs. [23, 39, 40]. The notations adopted here are also the same, but to make this paper self-contained, all the necessary definitions will be also presented below.

1. *$\pi\pi$ sector*

In this subsection, we briefly review the formulas of the scattering length used in the present work from two-particle energy in a finite box, with emphasis on the formula for the $I=0$ s-wave $\pi\pi$ system. Also we discuss the detailed procedure for extracting the energies of the $\pi\pi$ system. Here we follow the original derivations and notations in Refs. [36–38].

Let us consider the $\pi\pi$ system of two Nambu-Goldstone pions in the Asqtad-improved staggered dynamical fermion formalism. Using operators $\mathcal{O}_\pi(x_1)$, $\mathcal{O}_\pi(x_2)$, $\mathcal{O}_\pi(x_3)$, $\mathcal{O}_\pi(x_4)$ for pions at points x_1, x_2, x_3 and x_4, respectively, with the pion interpolating field operators defined by

$$\begin{aligned} \pi^+(t) &= -\sum_{\mathbf{x}} \bar{d}(\mathbf{x},t)\gamma_5 u(\mathbf{x},t) \\ \pi^-(t) &= \sum_{\mathbf{x}} \bar{u}(\mathbf{x},t)\gamma_5 d(\mathbf{x},t) \\ \pi^0(t) &= \frac{1}{\sqrt{2}}\sum_{\mathbf{x}} [\bar{u}(\mathbf{x},t)\gamma_5 u(\mathbf{x},t) - \bar{u}(\mathbf{x},t)\gamma_5 d(\mathbf{x},t)]. \end{aligned}$$

We then represent the $\pi\pi$ four-point functions as

$$C_{\pi\pi}(x_4,x_3,x_2,x_1) = \left\langle \mathcal{O}_\pi(x_4)\mathcal{O}_\pi(x_3)\mathcal{O}_\pi^\dagger(x_2)\mathcal{O}_\pi^\dagger(x_1)\right\rangle,$$

where $\langle\cdots\rangle$ represents the expectation value of the path integral, which we evaluate using the lattice QCD simulations.

In the current study, we only consider the dominant low energy states in the moving frame, which are the one pion with zero momentum, and one pion with the momentum $\mathbf{p}=(2\pi/L)\mathbf{e}_3$ (namely, $\mathbf{d}=\mathbf{e}_3$) and the total momentum $\mathbf{P}=\mathbf{p}$. The operator which creates a single pion with non-zero three momentum $\mathbf{k}$ from the vacuum is obtained by the Fourier transform:

$$\mathcal{O}_\pi(\mathbf{k},t) = \sum_{\mathbf{x}} \mathcal{O}_\pi(\mathbf{x},t) e^{i\mathbf{k}\cdot\mathbf{x}}\,. \tag{25}$$

After summing over the spatial coordinates $\mathbf{x}_1$, $\mathbf{x}_2$, $\mathbf{x}_3$ and $\mathbf{x}_4$, we obtain the $\pi\pi$ four-point function in the momentum $\mathbf{p}$ state,

$$C_{\pi\pi}(\mathbf{p},t_4,t_3,t_2,t_1) = \sum_{\mathbf{x}_1,\mathbf{x}_2,\mathbf{x}_3,\mathbf{x}_4} e^{i\mathbf{p}\cdot(\mathbf{x}_4-\mathbf{x}_2)} C_{\pi\pi}(x_4,x_3,x_2,x_1)\,, \tag{26}$$

where $x_1 \equiv (\mathbf{x}_1,t_1)$, $x_2 \equiv (\mathbf{x}_2,t_2)$, $x_3 \equiv (\mathbf{x}_3,t_3)$, and $x_4 \equiv (\mathbf{x}_4,t_4)$, and t stands for the time difference, namely, $t \equiv t_3 - t_1$.

To avoid the complicated Fierz rearrangement of quark lines, we used creation operators at time slices that are different by one lattice time spacing as it is suggested in Ref. [38], namely, we select $t_1=0, t_2=1, t_3=t$, and $t_4=t+1$.

In the $\pi\pi$ system, there are two isospin eigenstates, namely, $I=0$ and $I=2$, in this study, we only consider $I=0$ channel, we construct the $\pi\pi$ operators for this isospin eigenchannel as

$$\begin{aligned} \mathcal{O}_{\pi\pi}^{I=0}(\mathbf{p},t) = \frac{1}{\sqrt{3}}\Big\{ &\pi^-(t)\pi^+(\mathbf{p},t+1) + \pi^+(t)\pi^-(\mathbf{p},t+1) \\ &- \pi^0(t)\pi^0(\mathbf{p},t+1)\Big\}\,, \end{aligned} \tag{27}$$

where the $\mathbf{p}$ is the total momentum of the $\pi\pi$ system or the momentum of pion meson. This $\pi\pi$ operator has $(I,I_z)=(0,0)$.

If we assume that the u and d quarks have same mass, only four diagrams contribute to the $\pi\pi$ scattering amplitudes [36–38]. The quark line diagrams contributing to $\pi\pi$ four-point function are displayed in Fig. 1, labeling them as direct(D), crossed (C), rectangular (R), and vacuum (V) diagrams, respectively. The direct and crossed diagrams can be easily evaluated by constructing the corresponding four-point amplitudes for arbitrary values of t_3 and t_4 using only two wall sources placed at the fixed time slices t_1 and t_2. However, the rectangular (R) and vacuum diagrams (V), require another quark propagators connecting the time slices t_3 and t_4.

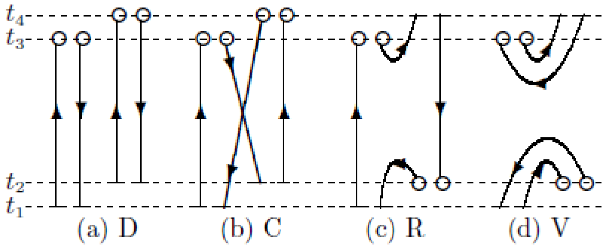

FIG. 1: Diagrams contributing to $\pi\pi$ four-point functions. Short bars stand for wall sources. Open circles are sinks for local pion operators.

Encouraged by the exploratory works of the $\pi\pi$ scattering at the $I=0$ channel [37, 38], and our reliable extraction of the $\pi\pi$ scattering length [24] at the $I=0$ channel with zero momentum, in the same way, we solve this problem by evaluating T quark propagators on a $L^3\times T$

lattice in the same way, each propagator, which corresponds to a wall source at the time slice $t = 0, \cdots, T-1$, are denoted by

$$\sum_{n''} D_{n',n''} G_t(n'') = \sum_{\mathbf{x}} \delta_{n',(\mathbf{x},t)}, \quad 0 \leq t \leq T-1, \quad (28)$$

where D is the quark matrix for the staggered Kogut-Susskind quark action. The combination of $G_t(n)$ that we apply for $\pi\pi$ four-point functions is shown in Fig. 1. For the non-zero momentum, we used an up quark source with 1, and an anti-up quark source with $e^{i\mathbf{p}\cdot\mathbf{x}}$ (except for D, where we use 1) on each site for two pion creation operator, respectively. D, C, R, and V, are schematically shown in Fig. 1, and we can express them in terms of the quark propagators G, namely,

$$\begin{aligned}
C_{\pi\pi}^{D}(\mathbf{p},t_4,t_3,t_2,t_1) &= \mathrm{Re}\sum_{\mathbf{x}_3}\sum_{\mathbf{x}_4} e^{i\mathbf{p}\cdot\mathbf{x}_4} \left\langle \mathrm{Tr}[G_{t_1}^{\dagger}(\mathbf{x}_3,t_3)G_{t_1}(\mathbf{x}_3,t_3)G_{t_2}^{\dagger}(\mathbf{x}_4,t_4)G_{t_2}(\mathbf{x}_4,t_4)]\right\rangle, \\
C_{\pi\pi}^{C}(\mathbf{p},t_4,t_3,t_2,t_1) &= \mathrm{Re}\sum_{\mathbf{x}_3}\sum_{\mathbf{x}_4} e^{i\mathbf{p}\cdot\mathbf{x}_4} \left\langle \mathrm{Tr}[G_{t_1}^{\dagger}(\mathbf{x}_3,t_3)G_{t_2}(\mathbf{x}_3,t_3)G_{t_2}^{\dagger}(\mathbf{x}_4,t_4)G_{t_1}(\mathbf{x}_4,t_4)]\right\rangle, \\
C_{\pi\pi}^{R}(\mathbf{p},t_4,t_3,t_2,t_1) &= \mathrm{Re}\sum_{\mathbf{x}_2}\sum_{\mathbf{x}_3} e^{i\mathbf{p}\cdot\mathbf{x}_2} \left\langle \mathrm{Tr}[G_{t_1}^{\dagger}(\mathbf{x}_2,t_2)G_{t_4}(\mathbf{x}_2,t_2)G_{t_4}^{\dagger}(\mathbf{x}_3,t_3)G_{t_1}(\mathbf{x}_3,t_3)]\right\rangle, \\
C_{\pi\pi}^{V}(\mathbf{p},t_4,t_3,t_2,t_1) &= \mathrm{Re}\sum_{\mathbf{x}_2}\sum_{\mathbf{x}_3} e^{i\mathbf{p}\cdot(\mathbf{x}_2-\mathbf{x}_3)} \left\langle \mathrm{Tr}[G_{t_1}^{\dagger}(\mathbf{x}_2,t_2)G_{t_1}(\mathbf{x}_2,t_2)G_{t_4}^{\dagger}(\mathbf{x}_3,t_3)G_{t_4}(\mathbf{x}_3,t_3)]\right\rangle, \qquad (29)
\end{aligned}$$

where daggers mean the conjugation by the even-odd parity $(-1)^n$ for the staggered Kogut-Susskind quark action, and Tr stands for the trace over color index. The hermiticity properties of propagator G are used to eliminate factors of γ^5. We know that when we calculate the disconnected part of the sigma correlator for the cases with non-zero momenta, the subtraction of the vacuum expectation value is not needed in Refs. [23, 39, 40]. Similarly, the vacuum diagram here is not accompanied by a vacuum subtraction for the cases with non-zero momenta.

As it is discussed in Refs. [37, 38], the rectangular and vacuum diagrams create gauge-variant noise. One can reduce the noise by fixing gauge configurations to some gauge (e.g., Coulomb gauge), and select a special wall source to emit only the Nambu-Goldstone pion [41], however, the gauge non-invariant states may contaminate the $\pi\pi$ four-point function. Alternatively, we perform the gauge field average without gauge fixing since the gauge dependent fluctuations should neatly cancel out among the lattice configurations. Besides these cancelations, the summation of the gauge-variant terms over the spatial sites of wall source further suppresses the gauge-variant noise. In this work we found that it works well.

All four diagrams in Fig. 1 are needed to study $\pi\pi$ scattering in the $I = 0$ channel. As it is investigated in Ref. [37], in the isospin limit, the $\pi\pi$ correlation function for $I = 0$ channel can be expressed as the combinations of four diagrams, namely,

$$C_{\pi\pi}(t) \equiv \langle \mathcal{O}_{\pi\pi}(t)|\mathcal{O}_{\pi\pi}(0)\rangle = D + \frac{1}{2}C - 3R + \frac{3}{2}V, \quad (30)$$

where the operator $\mathcal{O}_{\pi\pi}$ denoted in Eq. (27) creates a $\pi\pi$ state with total isospin 0.

In the usual manner, pion mass m_π can be evaluated through one-pole fitted functions

$$C_\pi(t) = \cosh\left[-m_\pi(t - T/2)\right] + \cdots. \quad (31)$$

In our concrete calculation we also evaluate the ratios

$$R^X(t) = \frac{C_{\pi\pi}^{X}(\mathbf{p},0,1,t,t+1)}{C_\pi(\mathbf{0},0,t)C_\pi(\mathbf{p},1,t+1)}, \quad X = D, C, R, \text{ and } V, \quad (32)$$

where $C_\pi(\mathbf{0},0,t)$ and $C_\pi(\mathbf{p},1,t{+}1)$ are the pion two-point functions with the momentum $\mathbf{0}$ and $\mathbf{p}$, respectively.

We should keep in mind that, for the staggered Kogut-Susskind quark action, there are further complications in itself stemming from the non-degeneracy of pions in the Goldstone and other channels at a finite lattice spacing. Briefly speaking, the contributions of non-Nambu-Goldstone pions in the intermediate states is exponentially suppressed for large times due to their heavier masses compared to these of the Nambu-Goldstone pion [36–38]. Therefore, we consider such $\pi\pi$ interpolator does not couple significantly to other $\pi\pi$ tastes, and neglect this systematic errors for the $\pi\pi$ sector.

2. σ sector

In our previous works [23, 39, 40], we make a detailed procedure to measure $\langle 0|\sigma^\dagger(t)\sigma(0)|0\rangle$. To simulate the correct number of quark species, we use the fourth-root trick, which automatically performs the transition from four tastes to one taste per flavor for staggered fermion at all orders. We employ an interpolation operator with isospin $I = 0$ and $J^P = 0^+$ at the source and sink,

$$\mathcal{O}(x) \equiv \sum_{a,g} \frac{\bar{u}^a_g(x) u^a_g(x) + \bar{d}^a_g(x) d^a_g(x)}{\sqrt{2 n_r}},$$

where g is the index of the taste replica, n_r is the number of the taste replicas, a is the color index, and we omit Dirac-spinor index. The time slice correlator $C(t)$ for σ meson in the momentum $\mathbf{p}$ state can be evaluated by

$$\begin{aligned} C(\mathbf{p}, t) = \frac{1}{n_r} \sum_{\substack{\mathbf{x},a,b \\ g,g'}} e^{i\mathbf{p}\cdot\mathbf{x}} \Big\{ & \langle \bar{u}^b_{g'}(\mathbf{x}, t) u^b_{g'}(\mathbf{x}, t) \bar{u}^a_g(\mathbf{0}, 0) u^a_g(\mathbf{0}, 0) \rangle \\ & + \langle \bar{u}^b_{g'}(\mathbf{x}, t) u^b_{g'}(\mathbf{x}, t) \bar{d}^a_g(\mathbf{0}, 0) d^a_g(\mathbf{0}, 0) \rangle \Big\}, \end{aligned} \tag{33}$$

where we consider u, d quarks are degenerate, and let $\mathbf{0}, \mathbf{x}$ be the spatial points of the σ state at source, sink, respectively. After performing Wick contractions of fermion fields, and summing over the taste index, for the light quark Dirac operator M, we obtain

$$\begin{aligned} C(\mathbf{p}, t) = & -\frac{1}{2} \sum_{\mathbf{x}} e^{i\mathbf{p}\cdot\mathbf{x}} \left\langle \mathrm{Tr} M^{-1}(\mathbf{x}, t; \mathbf{x}, t) \mathrm{Tr} M^{-1}(\mathbf{0}, 0; \mathbf{0}, 0) \right\rangle \\ & + \sum_{\mathbf{x}} (-)^x e^{i\mathbf{p}\cdot\mathbf{x}} \left\langle \mathrm{Tr}[M^{-1}(\mathbf{x}, t; \mathbf{0}, 0) M^{-1^\dagger} \mathbf{x}, t; \mathbf{0}, 0)] \right\rangle, \end{aligned} \tag{34}$$

where Tr is the trace over color index, and $x = (\mathbf{x}, t)$ is the lattice position. The first and second terms are the point-to-point quark-line disconnected contribution and connected contribution, respectively.

For staggered quarks, the meson propagators have the generic single-particle form,

$$\mathcal{C}(t) = \sum_i A_i e^{-m_i t} + \sum_i A'_i (-1)^t e^{-m'_i t} + (t \to N_t - t), \tag{35}$$

where the oscillating terms correspond to a particle with opposite parity. For the σ meson correlator, we consider only one mass with each parity in Eq. (35), namely, in our concrete calculation, our operator is the state with spin-taste assignment $I \otimes I$ and its oscillating term with $\gamma_0\gamma_5 \otimes \gamma_0\gamma_5$ [23, 39, 40]. Therefore, the σ correlator was then fit to the following physical model,

$$C_\sigma(t) = b_\sigma e^{-m_\sigma t} + b_{\eta_A} (-)^t e^{-M_{\eta_A} t} + (t \to N_t - t), \tag{36}$$

where the b_{η_A} and b_σ are two overlap factors. In Figure 4 we can clearly note this oscillating term.

We should understand that, for the staggered Kogut-Susskind quark action, our σ interpolator couples to various tastes as we examined in our previous study for the scalar a_0 and σ mesons [23, 39, 40], where we investigate the two-pseudoscalar intermediates states (namely, bubble contribution). Therefore, we should remove a number of the unwanted two-pseudoscalar intermediates states with different tastes and slightly different energies from the σ correlator.

3. *Off-diagonal sector*

To avoid the complicated Fierz rearrangement of the quark lines, we choose the creation operators at the time slices which are different by one lattice time spacing as it is suggested in Ref. [38], namely, we select $t_1 = 0, t_2 = 1$, and $t_3 = t$ for $\pi\pi \to \sigma$ three-point function, and choose $t_1 = 0, t_2 = t$, and $t_3 = t + 1$ for $\sigma \to \pi\pi$ three-point function.

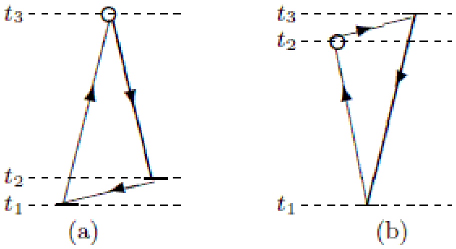

FIG. 2: Diagrams contributing to $\pi\pi \to \sigma$ and $\sigma \to \pi\pi$ three-point functions. Short bars stand for wall sources. Open circles are sinks for local pion operator. (a) Quark contractions of $\pi\pi \to \sigma$ and (b) Quark contractions of $\sigma \to \pi\pi$.

The quark line diagrams contributing to the $\sigma \to \pi\pi$ or $\pi\pi \to \sigma$ three-point function denoted in Eq. (24) are plotted in Fig. 2(a) and Fig. 2(b), respectively. The $\pi\pi \to \sigma$ three-point function can be easily evaluated by constructing the corresponding three-point amplitudes for arbitrary values of the time slice t_3 using only two wall sources placed at the fixed time slices t_1 and t_2. However, the calculation of $\sigma \to \pi\pi$ three-point function is almost the same difficult as that of the rectangular diagram for $\pi\pi$ four-point correlator function, because it requires another quark propagator connecting the time slices t_2 and t_3. For the nonzero momentum, we used an up quark source with 1, and an anti-up quark source with $e^{i\mathbf{p}\cdot\mathbf{x}}$ on each site for pion creation operator. The $\sigma \to \pi\pi$ and $\pi\pi \to \sigma$ three-point functions are schematically shown in Fig. 1, and we can also express them in terms of the quark propagators G, namely,

$$\begin{aligned} C_{\pi\pi\to\sigma}(\mathbf{p}, t_3, t_2, t_1) \; = & \\ \mathrm{Re} \sum_{\mathbf{x}_3, \mathbf{x}_1} e^{i\mathbf{p}\cdot\mathbf{x}_3} & \left\langle \mathrm{Tr}[G_{t_1}(\mathbf{x}_3, t_3) G^\dagger_{t_2}(\mathbf{x}_3, t_3) G^\dagger_{t_2}(\mathbf{x}_1, t_1)] \right\rangle, \\ C_{\sigma\to\pi\pi}(\mathbf{p}, t_3, t_2, t_1) \; = & \\ \mathrm{Re} \sum_{\mathbf{x}_2, \mathbf{x}_1} e^{i\mathbf{p}\cdot\mathbf{x}_2} & \left\langle \mathrm{Tr}[G_{t_1}(\mathbf{x}_2, t_2) G^\dagger_{t_3}(\mathbf{x}_2, t_2) G^\dagger_{t_3}(\mathbf{x}_1, t_1)] \right\rangle, \end{aligned} \tag{37}$$

D. Extraction of energies

Through calculating the matrix of correlation function denoted in Eq. (24), we can separate the ground state from first excited state in a clean way. It is very important to map out "avoided level crossings" between the σ resonance and its decay products in a finite box volume, because the first excited state is potentially close to the ground state. This makes the extraction of the ground state energy unfeasible if we only utilize a single exponential fit ansatz. Since we can not predict a priori whether our energy eigenvalues are near to the resonance region or not, we find it safe to adopt the correlation matrix to analyze our lattice simulation data. To extract the lowest two energy eigenstates, we follow the variational method [32] and construct a ratio of correlation function matrices as

$$M(t,t_R) = C(t)\,C^{-1}(t_R), \tag{38}$$

with some reference time slice t_R [42], which is assumed to be large enough such that the contributions to correlation matrix $M(t,t_R)$ from the excited states can be neglected, and the lowest two eigenstates dominate the correlation function. The two lowest energy levels can be extracted by a proper fit to two eigenvalues $\lambda_n(t,t_R)$ $(n=1,2)$ of matrix $M(t,t_R)$. Because here we work on the staggered fermion, and we can easily prove that $\lambda_n(t,t_R)$ $(n=1,2)$ behaves as [25, 43, 44]

$$\begin{aligned}\lambda_n(t,t_R) \;&=\; A_n \cosh\left[-E_n\left(t-\frac{T}{2}\right)\right] + \\ &(-1)^t B_n \cosh\left[-E_n'\left(t-\frac{T}{2}\right)\right],\end{aligned} \tag{39}$$

which explicitly contains an oscillating term, for a large t, which mean $0 \ll t_R < t \ll T/2$ to suppress the excited states and the unwanted thermal contributions. Here non-degenerate eigenvalues $\lambda_1(t,t_R) > \lambda_2(t,t_R)$ are assumed. In practice, the oscillating term in $\lambda_1(t,t_R)$ is not appreciable, we can also adopt following simple fitting model,

$$\lambda_1(t,t_R) = A\cosh\left[-E\left(t-\frac{T}{2}\right)\right], \tag{40}$$

and the difference between the fitting models of Eq. (39) and Eq. (40) is small.

III. LATTICE CALCULATION

A. Simulation parameters

We used the MILC lattices with 2+1 dynamical flavors of the Asqtad-improved staggered dynamical fermions, the detailed description of the simulation parameters can be found in Refs. [27, 28]. We analyzed the $\pi\pi$ four-point functions on the 0.15 fm MILC lattice ensemble of 360 $16^3 \times 48$ gauge configurations with bare quark masses $am_{ud} = 0.0097$ and $am_s = 0.0484$ and bare gauge coupling $10/g^2 = 6.572$, which has a physical volume approximately 2.5 fm. The inverse lattice spacing $a^{-1} = 1.358^{+35}_{-13}$ GeV [27, 28]. The mass of the dynamical strange quark is near to its physical value, and the masses of the u and d quarks are degenerate. Periodic boundary condition is applied to three spatial directions and temporal direction.

B. Sources

To calculate the $\pi\pi$ correlation functions, we use the standard conjugate gradient method (CG) to obtain the required matrix element of the inverse fermion matrix. The calculation of the correlation function for the rectangular diagrams naturally requires us to compute the propagators on all the time slices $t_s = 0, \cdots, T-1$ of both source and sink, which requires the calculation of 48 separate propagators in our lattice simulation. After averaging the correlator over all 48 possible values, the statistics are greatly improved since we can put the pion source at all possible time slices, namely, the correlator $C_{11}(t)$ is then calculated through

$$\begin{aligned}C_{11}(t) \;&=\; \left\langle (\pi\pi)\,(t)\,(\pi\pi)^\dagger\,(0)\right\rangle \\ &=\; \frac{1}{T}\sum_{t_s}\left\langle (\pi\pi)\,(t+t_s)\,(\pi\pi)^\dagger\,(t_s)\right\rangle,\end{aligned} \tag{41}$$

The best-effort to generate propagators on all the time slices allows us to obtain the correlators with high precision, which is very important to extract the desired scattering phase shifts reliably.

For each time slice, six fermion matrix inversions are required corresponding to the possible 3 color choices for two pion sources, and each inversion takes about one thousand iterations during the CG calculation. Therefore, all together we carry out 288 inversions for each valence quark mass on a given configuration. As shown follow, this large number of inversions, performed on 360 configurations, provides the substantial statistics needed to resolve the real part of the $I=0$ amplitude with reliable accuracy.

In the calculation of the off-diagonal correlator, $C_{21}(t)$, the quark line contractions results in a three-point diagram. Since in this three-point diagram two pion fields are located at the source time slice t_s, t_s+1, respectively. We calculate off-diagonal correlator $C_{21}(t)$ through

$$C_{21}(t) = \langle \sigma(t)(\pi\pi)^\dagger(0)\rangle = \frac{1}{T}\sum_{t_s}\langle \sigma(t+t_s)(\pi\pi)^\dagger(t_s)\rangle, \tag{42}$$

where, again, we sum the correlator over all time slices t_s and average it. As for the second off-diagonal correlator $C_{12}(t)$, two pion fields are placed at the sink time slices t_s+t and $t+t_s+1$, respectively, which make the computation of $C_{12}(t)$ difficult. However, using the relation $C_{12}(t) = C_{21}^*(t)$, we can obtain the off-diagonal matrix element C_{12} for free [45, 46]. The $\sigma \to \pi\pi$ component agrees with $\pi\pi \to \sigma$ within the error, but the statistical errors of the matrix element C_{12} should be larger than that of matrix element C_{21} for a large t. Therefore, in the following analysis we substitute matrix element C_{12} by the complex conjugate of matrix element C_{21}, which is not only to save about 20% computation time, but also significantly to reduce statistical errors.

For the σ correlator, $C_{22}(t)$, we have measured the point-to-point correlator with high precision in our previous work for the this lattice ensemble, therefore, we can just use the available propagators to construct the σ-correlator

$$C_{22}(t) = \left\langle \sigma^\dagger(t+t_s)\sigma(t_s)\right\rangle , \qquad (43)$$

where, also, we sum the correlator over all time slices t_s and average it. We must stress that we use Z_2 noisy estimators based on random color fields to measure the disconnected correlator [47]. To obtain the signals properly, we carry out numerical simulations with a high precision and careful analyses. In our previous work [47], we present the detailed procedures for the implementation of the Z_2 method. Using the method discussed in Ref. [48], we determine that 1000 noise Z_2 sources are sufficiently reliable.

One thing we must keep in mind that, in the calculation of the correlator $\langle(\pi\pi)(\pi\pi)^\dagger\rangle$, we make our best-efforts to reliably measure these rectangular and vacuum pieces, since the other two pieces are relatively easy to evaluate. We find that the rectangular and vacuum diagram make a major role in this correlator. Therefore, we get it properly for the $\pi\pi$ sector.

In this work, we also measure two-point correlator for pion, namely,

$$\begin{aligned} G_\pi(t;\mathbf{0}) &= \langle 0|\pi^\dagger(\mathbf{0},t)\pi(\mathbf{0},t_s)|0\rangle, \\ G_\pi(t;\mathbf{p}) &= \langle 0|\pi^\dagger(\mathbf{p},t)\pi(\mathbf{p},t_s)|0\rangle, \end{aligned} \qquad (44)$$

where the $G_\pi(t;\mathbf{0})$ and $G_\pi(t;\mathbf{p})$ is correlation function for the pion with the momentum $\mathbf{0}$ and $\mathbf{p}$, respectively.

IV. SIMULATION RESULTS

A. Time correlation function

In Fig. 3 the individual ratios, which are defined in Eq. (32) corresponding to the diagrams in Fig. 1, R^X $(X = D, C, R$ and $V)$ [1] are plotted as the functions of t. It is quite noisy for the disconnected diagram (V), but we can still get a good signal up to time separation $t = 14$. The calculations of the amplitudes for the rectangular and vacuum diagrams stand for our principal works. Clear signals observed up to $t = 20$ for the rectangular amplitude and up to $t = 14$ for the vacuum amplitude demonstrate that the method of wall source without gauge fixing used here is practically applicable.

The values of the direct amplitude R^D is quite close to unity, indicating that the interaction in this channel is very weak. The crossed amplitude, on the other hand, increases linearly, which implies a repulsion in this channel. After an initial increase up to $t \sim 4$, the rectangular amplitude exhibits a roughly linear decrease up to $t \sim 15$, and loss of signals after that, which suggests an attractive force between two pions. These features are what we eagerly expected from the theoretical predictions [36, 49]. We can observe that the crossed and rectangular amplitudes have the same value at $t = 0$, and the close values for small t. Because our analytical expressions in Eq. (29) for the two amplitudes coincide at $t = 0$, they should behave similarly until the asymptotic $\pi\pi$ state is reached.

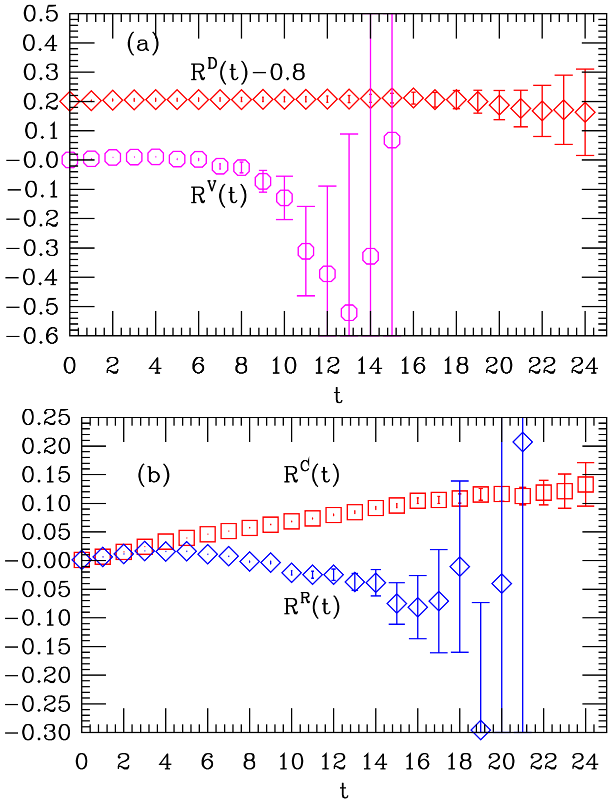

FIG. 3: (color online). Individual amplitude ratios $R^X(t)$ for $\pi\pi$ four-point function calculated by wall source as functions of t. Direct diagram shifted by 0.8 (diamonds), crossed diagram (octagons) and rectangular (squares) diagrams.

The vacuum amplitude is negligibly small up to $t \sim 8 - 14$, and loss of signals after that. This characteristic is in well accordance with the Okubo-Zweig-Iizuka (OZI) rule and χPT in leading order, which expects the disappearing of the vacuum amplitude [37]. Since its correlation functions reflect the quantum fluctuations of QCD vacuum, the errors for disconnected amplitudes should be approximately independent of time separation t, and hence increases exponentially like $e^{2m_\pi t}$. Therefore, the signals present in this correlation functions are quickly buried in the noise and it is very difficult to obtain proper information from large time separation.

In Fig. 4, we show the real parts of the diagonal components ($\pi\pi \to \pi\pi$ and $\sigma \to \sigma$) and the real part of the off-diagonal component $\pi\pi \to \sigma$ of the correlation function $C(t)$ in Eq. (24). Since $C(t)$ is a Hermitian matrix, hence, in the following analysis we substitute $\sigma \to \pi\pi$ by

---

[1] We can easily verify that when $t \ll T/2$, we can approximately estimate the energy shift δE from the ratio R^X.

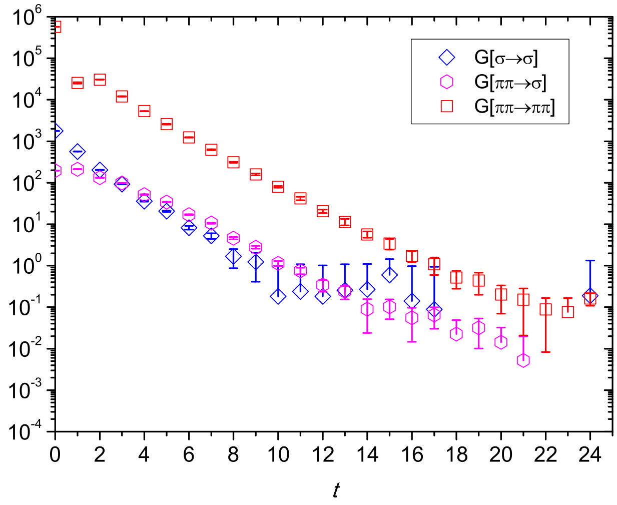

FIG. 4: (color online). Real part of the diagonal components ($\pi\pi \to \pi\pi$ and $\sigma \to \sigma$) and the real part of the off-diagonal component $\pi\pi \to \sigma$ of the time correlation function $C(t)$. Occasional points with negative central values for the off-diagonal component $\pi\pi \to \sigma$ and the diagonal component $\sigma \to \sigma$ are not displayed.

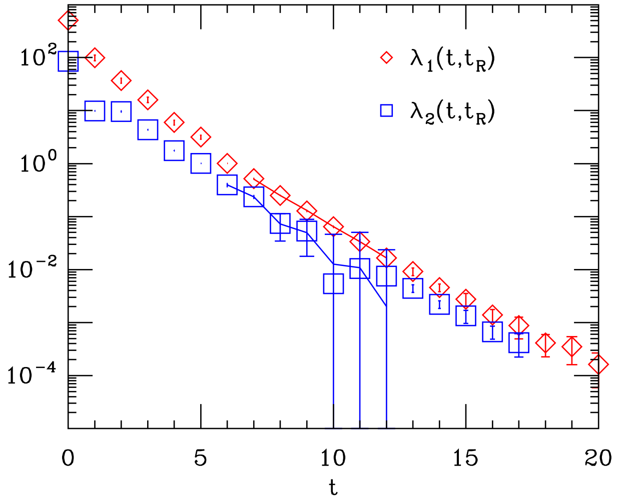

FIG. 5: (color online). The eigenvalues $\lambda_1(t,t_R)$ and $\lambda_2(t,t_R)$ as the function of t are shown. The solid lines are correlated fits to Eq. (39). Occasional points with negative central values for the correlator $\lambda_2(t,t_R)$ are not plotted.

$\pi\pi \to \sigma$ to reduce errors.

As we pointed out in Sec. II C 2, there exists bubble contribution in sigma correlator. In this work we will calculate the scattering phase shift with the bubble contribution removed from corresponding sigma correlator. In Ref. [39, 40], we presented the bubble term $B_\kappa(t)$, which was parameterized by three low-energy couplings μ, δ_A, and δ_V. In our concrete calculation, they were fixed to the values of our previous determinations [23, 40]. The taste multiplet masses in bubble terms were fixed as listed in Table 2 in Ref. [23]. After deducting the bubble term, the remaining sigma correlator now contains the clean information for sigma meson.

We calculate the two eigenvalues $\lambda_n(t,t_R)$ $(n=1,2)$ for the matrix $M(t,t_R)$ in Eq. (38) with the reference time $t_R = 6$. In Fig. 5 we plot our lattice results for $\lambda_n(t,t_R)(n=1,2)$ in a logarithmic scale for the moving frame, as a function of time t together with a correlated fit to the asymptotic form given in Eq. (39). From these fits we then extract the energies that will be used to determine the scattering phase.

To extract the energies reliably, we must take two major sources of systematic error into consideration. One arises from the excited states which affect the correlator in low time slice region. The other one stems from the thermal contributions which distort the correlator in high time slice region [50]. By denoting a fitting range $[t_{\min}, t_{\max}]$ and varying the values of the $t_{\min}$ and $t_{\max}$, we can control these systematic errors. In our concrete fitting, we take $t_{\min}$ to be t_R+1 and increase the reference time slice t_R to suppress the excited state contaminations. Moreover, we select $t_{\max}$ to be sufficiently far away from the time slice $t=T/2$ to avoid the unwanted thermal contributions. The corresponding fitting parameters t_R, $t_{\min}$ and $t_{\max}$ used in this work are tabulated in Table I. The corresponding fittings result in the reasonable values of χ^2/dof. The χ^2/dof together with the fit results for $\overline{E}_n$ $(n=1,2)$ are also listed in Table I.

TABLE I: The values of the energy eigenvalues for the ground state $(n=1)$ and the first excited state $(n=2)$. In the table we list the reference time t_R, the lower and upper bound of the fitting range, $t_{\min}$ and $t_{\max}$, the number of degrees of freedom (dof) for the fit quality χ^2/dof and the fit results for the energy eigenvalues $\overline{E}_n$ $(n=1,2)$ in lattice units.

n	t_R	$t_{\min}$	$t_{\max}$	$a\overline{E}_n$	χ^2/dof
1	6	7	12	0.6767(20)	0.922/2
2	5	6	12	0.8086(75)	0.158/3

The energy of the free pions E_1 is calculated from the mass m_π and energy E_π obtained by a single exponential fit to $G_\pi(t;\mathbf{0})$ and $G_\pi(t;\mathbf{p})$ in Eq. (44), as $E_1 = m_\pi + E_\pi$. These results are summarized in the upper part of Table II. We observe that $\overline{E}_1 < E_1 < \overline{E}_2$, which mean that the phase shift for $\lambda_1(t,t_R)$ and $\lambda_2(t,t_R)$ is positive and negative, respectively. This clearly indicates the existence of a resonance in between.

In Table III we show the mass m and the energy E of the pion and σ meson with momentum $\mathbf{p} = (2\pi/L)\mathbf{e}_3$, calculated from the corresponding time correlation functions. The σ meson with the zero momentum can not decay energetically, therefore, the mass and energy are extracted in a usual way [23].

TABLE II: The energy of $\pi\pi$ system $\overline{E}_n$ and the scattering phase shift δ. E_1^0 is the energy of the free pions. $\overline{E}_n$ is obtained from the fitting. The invariant mass $\sqrt{s}$, the the momentum k and the phase shifts δ calculated with the energy-momentum relations (47) in the continuum are referred to as *Cont*, and those obtained with the relations (48) on the lattice are referred to as *Lat*. The momentum k_0 is defined by $k_0^2 = s/4 - m_\pi^2$. All values with the mass dimension are in lattice units.

	$n = 1$		$n = 2$	
E_n^0	0.7085(6)		——	
$\overline{E}_n$	0.6767(20)		0.8086(38)	
	Cont	Lat	Cont	Lat
$\sqrt{s}$	0.5511(25)	0.5613(25)	0.7068(43)	0.7179(44)
k^2	0.0155(7)	0.0185(8)	0.0644(15)	0.0699(17)
k_0^2	——	0.0182(7)	——	0.0684(16)
$\tan\delta$	0.380(17)	0.257(14)	$-1.261(44)$	$-1.509(55)$
$\sin^2\delta$	0.126(9)	0.0621(64)	0.614(16)	0.695(15)

TABLE III: Mass m of the π and σ meson, and energy E of the π and σ meson with the momentum $\mathbf{p} = (2\pi/L)\mathbf{e}_3$, extracted from the time correlation function. All values are in lattice units.

	π	σ
m	0.2459(2)	0.594(35)
E	0.4626(5)	0.714(22)

B. Lattice discretization effects

In the continuum limit we have a dispersion relation

$$E = \sqrt{p^2 + m^2}, \tag{45}$$

for the single particle, which is particularly relevant for the finite-size methods used here [34]. On the lattice, this relation should be modified to [34]

$$\cosh(E) = 2 \cdot \sin^2(p/2) + \cosh(m). \tag{46}$$

We should consider the important discretization error in Rummukainen-Gottlieb formula (21). It arises from the Lorentz transformation from the moving frame to the center-of-mass frame using Lorentz symmetry in the continuum limit. In the Lorentz transformation we use these relations,

$$\begin{aligned} \sqrt{s} &= \sqrt{E_{MF}^2 - p^2}\,, \\ k^2 &= \frac{s}{4} - m_\pi^2, \end{aligned} \tag{47}$$

for the invariant mass $\sqrt{s}$, the energy in moving frame E_{MF} and the momentum k. However, on the lattice, the discretization effects explicitly break Lorentz symmetry and Eq. (47) is only valid up to the discretization errors. Therefore, the definitions of $\sqrt{s}$ and k contain the similar discretization errors, which have been extensively studied by Rummukainen and Gottlieb [34], and they suggest using the lattice modified relations, namely,

$$\begin{aligned} \cosh(\sqrt{s}) &= \cosh(E_{MF}) - 2\sin^2(p/2), \\ 2\sin^2(k/2) &= \cosh\left(\frac{\sqrt{s}}{2}\right) - \cosh(m_\pi), \end{aligned} \tag{48}$$

and hence the scattering phase shift is obtained by plugging the momentum k into the formula in Eq. (21).

To understand these discretization effects, in the present study we calculate the invariant mass $\sqrt{s}$ and the momentum k from the energy momentum relations both in the continuum (47) and on the lattice (48), and then estimate the corresponding phase shift by inserting the k into Eq. (21). We refer to the difference stemming from two choices as the discretization error, which should disappear in the continuum limit. The results for the invariant mass $\sqrt{s}$ (or E_{CM}), the momentum k and the phase shift δ are tabulated in Table II.

C. Extraction of resonance parameters

From Table II, we note that the considerable differences which depend on the chosen energy-momentum relations are obviously observed in $\sqrt{s}$ and k. Moreover, the thence difference for phase shift δ is significantly larger than the corresponding statistical errors. These are also shown in Fig. 6, where the phase shift $\sin^2\delta$, which is proportional to the scattering cross section of $\pi\pi$ system, is drawn. In Table II we see that the sign of the phase shift δ at $\sqrt{s} < m_\sigma$ ($am_\sigma = 0.594(33)$) is positive, which indicates an attractive interaction, and that at $\sqrt{s} > m_\sigma$ is negative, which suggests a repulsive interaction. These features are what we expected. It confirms the presence of a resonance at a mass around the σ mass m_σ.

In principle, it is straightforward to extract the σ meson decay width by fitting the phase shift data with the RBWF. However, the quark mass we studied here is significantly larger than its nature value, therefore a long chiral extrapolation is required. Since the kinematic factors in the decay width depend explicitly on the quark mass [22], and we just made a lattice simulation on one set of the quark mass, we have to avert this direct measurement of the decay width and adopt an alternative approach. As we discussed in Section II A, we parametrize the resonant characteristic of the s-wave phase shift δ_0 in terms of the effective $\sigma \to \pi\pi$ coupling constant $g_{\sigma\pi\pi}$, namely,

$$\tan\delta_0 = \frac{g_{\sigma\pi\pi}^2}{8\pi} \frac{k}{\sqrt{s}(M_R^2 - s)}, \tag{49}$$

where M_R is the resonance mass and $g_{\sigma\pi\pi}$ is denoted through the lagrangian

$$L_{\text{eff}} \sim g_{\sigma\pi\pi}\, \sigma\pi\pi, \tag{50}$$

as in the continuum theory. According to the discussions in Ref. [22], we can reasonably assume that the coupling constant $g_{\sigma\pi\pi}$ vary rather slowly as the quark mass changes. Thus, the equation (49) allows us to solve for two unknown parameters, namely, the coupling constant $g_{\sigma\pi\pi}$, and the σ meson mass m_σ.

The invariant mass $\sqrt{s}$ and the momentum k appearing in the continuum effective theory in Eq. (49) satisfy the energy-momentum relations (47). The thence discretization error may arise in the choice of $\sqrt{s}$ and k in the application of Eq. (49) to the extracted phase shift. Fortunately, our lattice results show that this does not cause a serious problem numerically. In Table II we also present the momentum k_0 evaluated by $k_0^2 = s/4 - m_\pi^2$ for a given $\sqrt{s}$, and m_π. We can notice that the difference between k and k_0 is not remarkable. Therefore, the error stemmed from the different definitions of the scattering momentum can be reasonably ignored. In practice, we employ the scattering momentum k_0 upon the application of Eq. (49).

The lattice simulation results of the coupling constant $g_{\sigma\pi\pi}$ and the resonance mass M_R solved by Eq. (49) are

$$\begin{aligned} g_{\sigma\pi\pi} &= 3.22(52)\,\mathrm{GeV}\,, \\ M_R &= 0.660(31)\,, \\ M_R/m_\sigma &= 1.112(85)\,, \end{aligned} \tag{51}$$

where we utilize the energy-momentum relations (47) in the continuum, and the σ meson mass m_σ is extracted from the corresponding correlation function in our previous study. If we employ the energy momentum relations (48) on the lattice, we obtain the corresponding simulation results as

$$\begin{aligned} g_{\sigma\pi\pi} &= 2.69(44)\,\mathrm{GeV}\,, \\ M_R &= 0.691(37)\,, \\ M_R/m_\sigma &= 1.163(93)\,. \end{aligned} \tag{52}$$

The value of coupling constant $g_{\sigma\pi\pi}$ is in reasonable agreement with $g_{\sigma\pi\pi} = 2.47(45)\,\mathrm{GeV}$ obtained in Ref. [51], $g_{\sigma\pi\pi} = 2.97(4)\,\mathrm{GeV}$ obtained in Ref. [52] and $g_{\sigma\pi\pi} = 2.86\,\mathrm{GeV}$ given in Ref. [22].

In Fig. 6, we display the curves for $\sin^2\delta_0$ obtained by Eq. (49) with the coupling constant $g_{\sigma\pi\pi}$ and the resonance mass M_R given in Eq. (51) and Eq. (52), respectively. The position at $\sin^2\delta_0 = 1$ which stand for the resonance mass M_R is also displayed in Fig. 6 for two cases (black cross and red plus for the continuum and lattice case, respectively). For visualized comparison, we also draw the sigma mass m_σ (fancy cyan plus). We can note that M_R is in reasonable agreement with the sigma mass m_σ.

Assuming that the dependence of $g_{\sigma\pi\pi}$ on quark mass is small [22], we can roughly estimate the σ meson decay width at the physical quark mass as

$$\Gamma^{\rm phy} = \frac{g_{\sigma\pi\pi}^2}{8\pi}\frac{k^{\rm phy}}{(m_\sigma^{\rm phy})^2}\,, \tag{53}$$

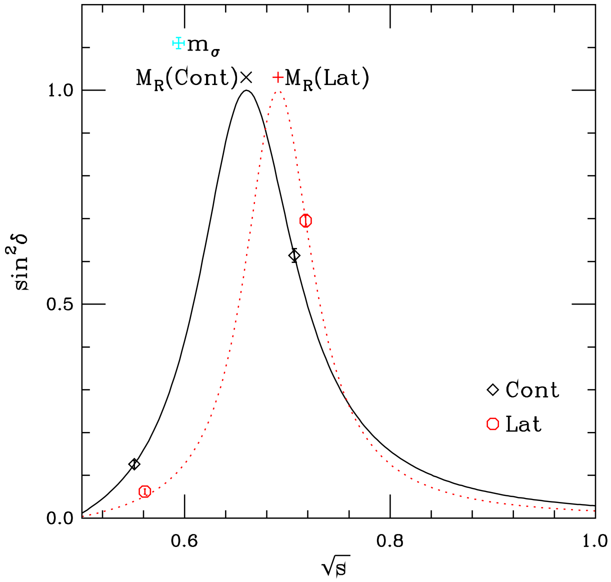

FIG. 6: (color online). The scattering phase shift $\sin^2\delta$, positions of σ mass m_σ and resonance mass M_R. **Cont** refer to the results achieved with the energy momentum relations in the continuum limit(47) and **Lat** to those with the relations on the lattice (48). The two lines are obtained by Eq. (49) with parameters $g_{\sigma\pi\pi}$ and M_R given in Eq. (51) and Eq. (52), respectively. The abscissa is in lattice units.

where $m_\sigma^{\rm phy} = 513 \pm 32$ MeV is the estimated physical σ meson mass taken from PDG [1], and momentum $k^{\rm phy}$ is calculated by

$$(k^{\rm phy})^2 = \frac{(m_\sigma^{\rm phy})^2}{4} - (m_\pi^{\rm phy})^2\,,$$

where $m_\pi^{\rm phy}$ is physical pion mass ($m_\pi^{\rm phy} \approx 140$ MeV) [1]. This produces

$$\Gamma^{\rm phy} = (337 \pm 82)\,\mathrm{MeV} \tag{54}$$

where we use the data given in Eq. (51), and

$$\Gamma^{\rm phy} = (236 \pm 49)\,\mathrm{MeV} \tag{55}$$

where we employ the data given in Eq. (52). We can observe that the difference stemming from our two chosen energy-momentum relations is comparable with the statistical error. Although our preliminary estimates for the $\sigma \to \pi\pi$ decay width in this work is not within the PDG estimated result $\Gamma = 600 - 1000$MeV [1], this is still an inspiring result, considering that we make a big assumption that the coupling constant does not depend on the quark mass, and we perform a long chiral extrapolation, etc.

In the present study, we make an extensive use of the relativistic Breit Wigner formalism, and the sigma meson is a very wide object and the RBWF approximation holds perfectly for relatively narrower objects. As it discussed in Ref. [53], we should adopt a much more model-independent approach to the extraction of the finite volume limit. In our future tasks, we must address the phenomenological treatment.

Bearing in mind that this work is an exploratory study, the main purpose is to present some conceptual issues of determining σ resonance parameters directly from lattice QCD calculations, we think that it is enough justified all these above assumptions and simplifications.

V. CONCLUSIONS AND OUTLOOKS

In the present work, we have carried out a direct lattice QCD calculation of the s-wave $\pi\pi$ scattering phase shift for the isospin $I = 0$ channel near the σ-meson resonance region at total non-zero momentum in the moving frame, where the rectangular graph and vacuum diagram play a key role, for the MILC "medium" coarse ($a = 0.15$ fm) lattice ensemble in the presence of $2 + 1$ flavors of the Asqtad improved staggered dynamical sea quarks. We employed the same technique in Ref. [37, 38], which we use the moving pion wall source operators without gauge fixing for the $I = 0$ channel to obtain the reliable precision. We calculated all the four diagrams which are categorized in Ref. [37, 38], and observed a clear signal of the attraction for $I = 0$ channel.

We have demonstrated that the calculation of the s-wave scattering phase shift for the $I = 0$ $\pi\pi$ system and then the estimation of the decay width of σ meson are practicable on the lattice QCD with our current limited computing resources. The phase shift data clearly shows the presence of a resonance at a mass around the σ meson mass obtained in our previous study [23]. This resonance can be reasonably identified with the σ meson. Moreover, we extracted the σ meson decay width from the phase shift data and showed that it is fairly compared with the estimated σ meson decay width from PDG [1].

However, we realize some important issues which should be cleared in the future works. One is to reduce the discretization errors, which we show in the previous section are significantly larger than the corresponding statistical errors. A simple way to solve this problem is to use a lattice configuration closer to the continuum limit. Moreover, a full analysis to determine the size dependence of the phase shift employing a set of lattice sizes is also highly desired. However, all of these issues are beyond the scope of this paper since this will require a substantial amount of computing resources. We leave these challenging tasks in our future study.

We adopted the effective range formula, which allows us to use the effective $\sigma \to \pi\pi$ coupling constant $g_{\sigma\pi\pi}$ to extrapolate from our lattice simulation point $m_\pi/m_\sigma \approx 0.414$ to the physical point $m_\pi/m_\sigma \approx 0.273$, assuming that $g_{\sigma\pi\pi}$ does not depend on the quark mass. This is just a rough estimation, thus a more direct evaluation of the decay width is highly desirable. As we pointed above, the decay width can be estimated directly from the energy dependence of the phase shift data by fitting the BWRF if we make the lattice simulations near to the physical quark mass and we have simulation data which have several energy near the resonance mass as it was done for the calculation of the ρ meson decay width in Ref. [50]. We will continue to look for the possible computational resources to accomplish this task.

When our preliminary lattice results obtained are compared with the corresponding PDG quantities, it is clear that the lattice QCD simulations can not yet match the accuracy of PDG, and even can not be considered to be"physical" one. Although a precise determination of the σ resonance parameters on the lattice is absolutely a big challenge, our preliminary work reported here can serve as stepping out the first step in an attempt to understand the strong σ decay from direct lattice QCD in a conceptually clean way.

Acknowledgments

This work is supported in part by the Fundamental Research Funds for the Central Universities (2010SCU23002) and the Startup Grant from the Institute of Nuclear Science and Technology of Sichuan University. We thank Carleton DeTar for kindly providing us the MILC gauge configurations used for this work and the fitting software to analyze the lattice simulation data. We are indebted to MILC Collaboration for using the Asqtad lattice ensemble and MILC codes. We are grateful to Hou Qing for his comprehensive supports. The computations for this work were carried out at AMAX, CENTOS and HP workstations in the Institute of Nuclear Science and Technology, Sichuan University.

---

[1] K. Nakamura *et al.* (Particle Data Group), J. Phys. G **37**, 075021 (2010).
[2] F. Ambrosino *et al.* [KLOE Collaboration], Eur. Phys. J. C **49**, 473 (2007).
[3] M. Ablikim *et al.* [BES Collaboration], Phys. Lett. B **645**, 19 (2007).
[4] M. Ablikim *et al.* [BES Collaboration], Phys. Lett. B **598**, 149 (2004).
[5] H. Muramatsu *et al.* [CLEO Collaboration], Phys. Rev. Lett. **89**, 251802 (2002) [Erratum-ibid. **90**, 059901 (2003)].
[6] M. Ishida, S. Ishida, T. Komada and S. I. Matsumoto, Phys. Lett. B **518**, 47 (2001).
[7] E. M. Aitala *et al.* [E791 Collaboration], Phys. Rev. Lett. **86**, 770 (2001).
[8] D. M. Asner *et al.* [CLEO Collaboration], Phys. Rev. D **61**, 012002 (2000).
[9] I. G. Alekseev, P. E. Budkovsky, V. P. Kanavets, L. I. Ko-

roleva, I. I. Levintov, V. I. Martynov, B. V. Morozov and V. M. Nesterov *et al.*, Phys. Atom. Nucl. **61**, 174 (1998) [Yad. Fiz. **61**, 223 (1998)] [Nucl. Phys. B **541**, 3 (1999)].

[10] Y. .A. Troian, E. B. Plekhanov, V. N. Pechenov, A. Y. .Troian, S. G. Arakelian and A. P. Jerusalimov, JINR Rapid Commun. **5-91**, 33 (1998).

[11] M. Svec, Phys. Rev. D **53**, 2343 (1996).

[12] T. Hyodo, D. Jido and T. Kunihiro, Nucl. Phys. A **848**, 341 (2010).

[13] G. Mennessier, S. Narison and X. G. Wang, Phys. Lett. B **688**, 59 (2010).

[14] Y. M. Zheng, C. Fuchs, P. Srisawad, A. Faessler, Y. P. Yan, C. Kobdaj and Y. Z. Xing, Commun. Theor. Phys. **50**, 725 (2008).

[15] I. Caprini, Phys. Rev. D **77**, 114019 (2008).

[16] F. J. Yndurain, R. Garcia-Martin and J. R. Pelaez, Phys. Rev. D **76**, 074034 (2007).

[17] I. Caprini, G. Colangelo and H. Leutwyler, Phys. Rev. Lett. **96**, 132001 (2006).

[18] Igi K and Hikasa K I, 1999 *Phys. Rev.* D **59** 034005.

[19] R. Escribano, A. Gallegos, J. L. Lucio M, G. Moreno, J. Pestieau, Eur. Phys. J. **C28**, 107 (2003).

[20] F. Giacosa and G. Pagliara, Phys. Rev. C **76**, 065204 (2007).

[21] J. R. Pelaez, Mod. Phys. Lett. A **19**, 2879 (2004).

[22] J. Nebreda and J. R. Pelaez, Phys. Rev. D **81**, 054035 (2010).

[23] Z. W. Fu, Chin. Phys. Lett. **28** 081202 (2011).

[24] Z. Fu, Commun. Theor. Phys. **57**, 78 (2012).

[25] Z. Fu, JHEP **1201**, 017 (2012).

[26] Z. Fu, Phys. Rev. D **85**, 014506 (2012).

[27] C. Bernard *et al.*, Phys. Rev. D **83**, 034503 (2011).

[28] A. Bazavov *et al.*, Rev. Mod. Phys. **82**, 1349 (2010).

[29] M. Luscher, Commun. Math. Phys. **105**, 153 (1986).

[30] M. Luscher, Nuclear Physics B **354**, 531 (1991).

[31] L. Lellouch and M. Luscher, Commun. Math. Phys. **219**, 31 (2001).

[32] M. Luscher and U. Wolff, Nucl. Phys. B **339**, 222 (1990).

[33] M. Luscher, Nucl. Phys. B **364**, 237 (1991).

[34] K. Rummukainen and S. A. Gottlieb, Nucl. Phys. B **450**, 397 (1995).

[35] T. Yamazaki *et al.*, Phys. Rev. D **70**, 074513 (2004).

[36] S. R. Sharpe, R. Gupta and G. W. Kilcup, Nucl. Phys. B **383**, 309 (1992).

[37] Y. Kuramashi, M. Fukugita, H. Mino, M. Okawa and A. Ukawa, Phys. Rev. Lett. **71**, 2387 (1993).

[38] M. Fukugita, Y. Kuramashi, M. Okawa, H. Mino and A. Ukawa, Phys. Rev. D **52**, 3003 (1995).

[39] C. Bernard, C. E. DeTar, Z. Fu and S. Prelovsek, Phys. Rev. D **76**, 094504 (2007).

[40] Z. W. Fu and C. DeTar, Chin. Phys. C **35** (2011) 896.

[41] R. Gupta, G. Guralnik, G. W. Kilcup and S. R. Sharpe, Phys. Rev. D **43**, 2003 (1991).

[42] M. Lüscher and U. Wolff, Nucl. Phys. B **339**, 222 (1990).

[43] A. Mihály, H. R. Fiebig, H. Markum and K. Rabitsch, Phys. Rev. D **55**, 3077 (1997).

[44] A. Mihály, "Studies of Meson-Meson Interactions within Lattice QCD", PhD thesis, Lajos Kossuth University, Debrecen, 1998.

[45] S. Aoki *et al.* (CP-PACS Collaboration), Phys. Rev. **D76**, 094506 (2007).

[46] S. Aoki *et al.* [CS Collaboration], Phys. Rev. D **84**, 094505 (2011).

[47] Z. Fu, "Hybrid meson decay from the lattice," PhD thesis, UMI-32-34073, University of Utah, Salt Lake city, 2006.

[48] Muroya S, Nakamura A, Nonaka C, Sekiguchi N and Wada H Nucl. Phys. Proc. Suppl. **106** 272 (2002).

[49] V. Bernard, N. Kaiser and U. G. Meissner, Nucl. Phys. B **357**, 129 (1991).

[50] X. Feng, K. Jansen and D. B. Renner, Phys. Rev. D **83**, 094505 (2011).

[51] R. Kaminski, G. Mennessier and S. Narison, Phys. Lett. B **680**, 148 (2009).

[52] J. A. Oller, Nucl. Phys. **A 727**, 353 (2003).

[53] M. Doring and U. G. Meissner, JHEP **1201**, 009 (2012).